Appl Magn Reson (2013) 44:189–201
DOI 10.1007/s00723-012-0393-y

Applied
Magnetic Resonance

Melting of Naphthalene Confined in Mesoporous Silica MCM-41

Bob Grünberg · Anna Grünberg · Hans-Heinrich Limbach · Gerd Buntkowsky

Received: 12 July 2012 / Published online: 23 September 2012

Abstract The ^{2}H nuclear magnetic resonance (NMR) solid-echo spectra of naphthalene molecules as guests in the mesopores of neat MCM-41 with a pore width of 3.3 nm were measured in the temperature regime from 180 to 250 K. A strong reduction of the melting point of the naphthalene molecules by 152 K is observed. The line shape changes in the melting region were simulated with two different models, namely, the model of a narrow distribution of activation energies, which is typical for a crystal-like phase, and a two-phase model. Both models indicate a relatively narrow distribution of melting points of the naphthalene molecules inside the pores, indicative of a rather well-defined structure of the naphthalene molecules inside the pores. This finding supports the proposal of a plastic crystalline phase previously proposed by other groups.

1 Introduction

Already in their bulk phases molecular solids offer a great richness of structural diversity and physico-chemical phenomena. A major reason is that the behavior of these materials is mainly controlled by the presence of—compared with ionic or covalent solids—relatively weak intermolecular interactions such as hydrogen bonding, dipolar interactions, π-stacking interactions or van-der-Waals interactions [1, 2]. The structural and dynamical properties of these materials become even more rich, if they are confined inside small pores, as for example in mesoporous environments. Typical examples are a very strong lowering of the melting point or

A. Grünberg · G. Buntkowsky (✉)
Eduard-Zintl-Institut für Anorganische und Physikalische Chemie, Technische Universität Darmstadt, Petersenstrasse 20, 64287 Darmstadt, Germany
e-mail: gerd.buntkowsky@chemie.tu-darmstadt.de

B. Grünberg · H.-H. Limbach
Institut für Chemie und Biochemie, Freie Universität Berlin, Takustr. 3, 14195 Berlin, Germany

even the formation of an amorphous, glass-like phase with a glass-transition instead of a regular melting [3–14]. For example, benzene [15] confined inside mesoporous silica exhibits different phases, which can be identified as a glass-like amorphous surface phase and an inner crystalline phase with properties close to solid bulk benzene; pyridine confined inside mesoporous silica exhibits a strong physisorbed surface phase due to hydrogen bonding of the silanol groups with the ring nitrogen [16, 17] and weakly bound inner molecules; a similar result is found for water-molecules [18, 19] or iso-butyric acid confined in mesoporous silica materials [20–23], or biphenyl inside silylated MCM-41, which reveals a glass-like amorphous surface phase with a characteristic pre-melting behavior below the glass-transition temperature [24].

In the present work the dynamic properties of naphthalene confined in mesoporous silica MCM-41 is investigated (Fig. 1). The crystal structure of bulk naphthalene was first solved by Robertson [25] and later refined by Abrahams and Robertson [26, 27] and Cruickshank [28]. It is a typical molecular crystal with a well-defined monoclinic rigid lattice structure where the molecules are arranged in a herringbone configuration with two inequivalent molecules in the unit cell [1]. Its lattice-parameters are $a = 8.235$ Å, $b = 6.003$ Å and $c = 8.685$ Å and $\beta = 122.9°$. Its melting point in the bulk phase is 80.3 °C.

Solid naphthalene is not exactly one of the most solid-state nuclear magnetic resonance (NMR)-friendly systems. In the crystal phase it exhibits only very slow molecular reorientations, due to a relatively high activation barrier. By proton NMR measurements of Strange et al. [29] determined a barrier height of (91 ± 7) kJ/mol for molecular reorientations, which they attributed tentatively to an in-plane motion of the naphthalene molecules. Earlier measurements by von Schütz and Wolf [30] have reported a similar value of (105 ± 8) kJ/mol. Owing to these high activation energy barriers relatively long T_1-times are expected. A simple estimation shows that for deuterons at room temperature T_1-times on the order of several hours to days are expected. For this reason detailed solid-state NMR studies of systems like solid naphthalene are only feasible, employing special hyperpolarization techniques, as

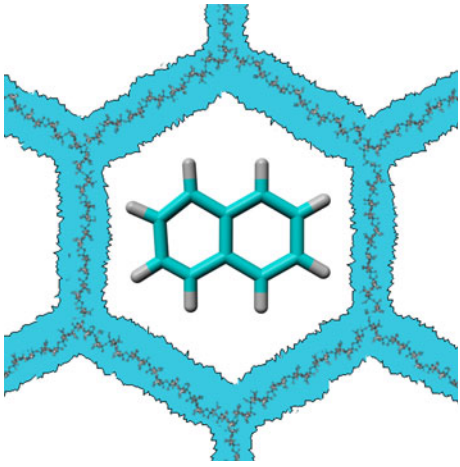

Fig. 1 Dynamics of napthalene-d_8 inside of mesoporous silica MCM-41 is studied by ^{2}H-solid-echo NMR spectroscopy

for example optical nuclear polarization (ONP, [31, 32]) enhanced ^{2}H or ^{13}C-solid-state NMR spectroscopy, which was pioneered by the Vieth group in Berlin [33–39], which are not generally available.

However, already in the early 1990s the Günther group found in a series of seminal NMR studies on naphthalene ball-milled in silica materials [40–43] that the melting point of naphthalene is strongly reduced in the confinement. Later, the Strange group has measured the proton-relaxation times (T_1, $T_{1\rho}$, T_2) of naphthalene confined in porous silica materials of various diameters [44], ranging from 4 to 50 nm in the temperature regime from 233 to 363 K on a 23.5-MHz NMR spectrometer. In their experiments they found a pronounced dependence of the relaxation times on the temperature, indicating a biphasic behavior of the naphthalene inside the pores, which they interpreted as the coexistence of crystalline naphthalene phase inside the pores and a plastic naphthalene phase in the pores. This interpretation was later supported by Huang and coworkers [45], which studied the phase behavior of naphthalene in mesoporous silica by differential scanning calorimetry, powder X-ray diffraction and Raman spectroscopy. From their X-ray data they concluded that the structure of the crystalline phase inside the pores is similar to the structure of the bulk-naphthalene.

Since a plastic phase is not known for bulk naphthalene and as we observed in previous ^{2}H solid-echo NMR studies of benzene inside mesoporous silica the coexistence of a crystalline and an amorphous benzene phase inside the pores, the above studies prompted us to take a deeper look at the nature of the plastic phase, employing variable temperature ^{2}H solid-echo NMR spectroscopy.

To be able to observe only the plastic phase we chose to employ narrow pore radius MCM-41 silica as carrier material for the naphthalene. Materials like MCM-41 or SBA-15 belong to a class of periodic mesoporous silica (PMS) materials, which was originally envisioned by Beck et al. [46]. They have high porosity, controllable and narrowly distributed pore sizes, high thermal stability [47] and the possibility of modifying and functionalizing the pore surface [48]. In these materials, the self-aggregation of structure directing surfactant molecules to micelles of specific shapes creates their characteristic morphology [49]. MCM-41 in particular has cylindrical pores arranged in hexagonal array and exhibits a narrow pore size distribution in the range from 2 to 10 nm. The actual pore diameter of a sample is determined by the diameter of the micelles in the template solution. The latter is controlled by selecting by the length of the alkyl-chains of the applied tenside.

MCM-41 has a high specific BET (Brunauer, Emmett, Teller [50]) surface area of typically 1,000 m^2/g and a specific pore volume of ca. 1 cm^3/g. This large surface areas and pore volumes allow the direct observation of molecules adsorbed on the surface or confined in the pores employing bulk techniques like solid-state NMR spectroscopy [47]. A characteristic property of MCM-41 is its relatively smooth pore surface [51, 52]. PMS are ideal model environments for the investigation of basic interactions between surfaces and substrates and confinement effects because they have both well-defined pore-diameters and chemically modifiable surfaces (for details see reviews [53, 54] and references therein).

In the present case, our strategy employs the differences in the temperature dependence of the solid-echo spectra on the activation energy distribution inside the samples. In particular, there are two limiting cases, which correspond to a crystal or to an amorphous glass-like state. If the distribution of these activation energies is very narrow, which is typical for a crystalline material (narrow distribution model), the molecules exhibit a well-defined melting-point and melting enthalpy. If $(\gamma_{cw} - \gamma_{lw})$ is the difference of the surface free energies γ_{cw} (crystal-wall) and γ_{lw} (liquid-wall), $T_{m(bulk)}$ the bulk melting temperature, V_m the molar volume of the liquid phase, ΔH_m the molar enthalpy of melting and R the universal gas constant, a linear dependence of the melting point depression ΔT_m on the inverse pore radius $1/R$ is expected. This relation is the Gibbs–Thomson equation [55]:

$$\Delta T_m = T_{m(bulk)} - T_{m(pore)} = \frac{2V_m T_{m(bulk)}(\gamma_{cw} - \gamma_{lw})}{\Delta H_m R}. \quad (1)$$

Following the initial development of ^{2}H Fourier transform solid-state NMR spectroscopy, the analysis of line shape changes in one- [56] and two-dimensional ^{2}H NMR spectra [57–60] has become the tool of choice for the analysis of molecular motions and reorientations in solid organic materials. Its theory in the presence of molecular motions is well known (see textbooks [61, 62]). The quadrupole coupling determines the positions of the two spin-transitions of an individual deuteron

$$\upsilon_Q(\vartheta, \varphi) = Q_{zz}\frac{1}{2}\left(3\cos^2\vartheta - 1 - \eta\sin^2\vartheta\cos 2\varphi\right) \quad (2)$$

with

$$Q_{zz} = \frac{3}{4}\frac{eQeq}{h} = \frac{3}{4}Q_{cc}, \quad (3)$$

where Q_{cc} is the quadrupolar coupling constant, eQ the electric quadrupole moment, eq represents the principle component of the EFG tensor, η is the asymmetry parameter, which is related to the shape of the electric field gradient and Q_{zz} characterizes the strength of the quadrupolar interaction. φ and ϑ are the azimuth- and polar angles of the quadrupolar principal axis system (PAS) with respect to the external magnetic field B_0. In a non-oriented powder sample the average over all possible orientations has to be calculated by integration over the polar angles ϑ and φ, yielding the well-known Pake pattern.

From the point of view of ^{2}H solid-state NMR spectroscopy, which observes rotational motions of the molecules, the activation energies of reorientations are monitored. In the case of the narrow distribution model, the spectrum exhibits typical features in the transition from slow jumps ($k \ll Q_{cc}$) to fast jumps ($k \gg Q_{cc}$) which depend on the geometry of the jump process, with an Arrhenius-like dependence on the temperature. Analyzing this temperature dependence yields the activation energy of the motion.

The second limiting case is a broad distribution of activation energies, which is typically found in glass-like amorphous cases. In this situation, the spectra with exchange rates in the intermediate ($k \approx Q_{cc}$) regime contribute only to a negligible

fraction to the ^{2}H NMR spectrum and the ^{2}H NMR line shape is a weighted superposition of the line shapes for slow and fast jumps [63]. Since only the slow and the fast molecules are visible in the spectrum, this case is called the two-phase model. A characteristic of the model is the coexistence of the two phases with their individual quadrupolar coupling constants and varying relative intensities of each phase. A detailed analysis of this situation in the case of small organic glass-forming molecules was developed by Roessler et al. [63]. They could show that the relative concentrations of the two phases can be written as a shifted Gauss error-function, which is zero at low temperatures and one at high temperatures:

$$\begin{aligned} c_{\mathrm{A}}(T) &= \frac{1}{2}\mathrm{erf}\left(\frac{1}{\sqrt{2}\Delta T}(T - T_0)\right) + \frac{1}{2}\mathrm{erf}\left(\frac{1}{\sqrt{2}\Delta T}T_0\right), \\ c_{\mathrm{B}}(T) &= 1 - c_{\mathrm{A}}(T), \end{aligned} \tag{4}$$

where erf(x) is the Gaussian error-function

$$\mathrm{erf}(x) = \frac{2}{\sqrt{\pi}}\int_0^x \exp(-t^2)\mathrm{d}t. \tag{5}$$

From this expression, Roessler et al. [63] developed the distribution of activation energies in temperature units by differentiation of the concentration with respect to the temperature

$$g(T) = \frac{\mathrm{d}}{\mathrm{d}T}c_{\mathrm{A}}(T) = \frac{1}{\sqrt{2\pi}\Delta T}\exp\left(-\frac{(T - T_0)^2}{2\Delta T^2}\right). \tag{6}$$

This expression can be approximately converted into the distribution of activation energies by assuming an Arrhenius dependence between the characteristic activation energy, the temperature and the correlation times of the jump process:

$$E(T) = \ln\left(\frac{\tau(T)}{\tau_\infty}\right)k_{\mathrm{B}}T = \alpha T. \tag{7}$$

Since the proportionality factor α depends only logarithmically on the ratio of $\tau(T)$ and τ_∞, it can be estimated assuming a typical vibrational correlation time of $\tau_\infty = 1 \times 10^{-13}$ s for the latter [63] and a characteristic value τ^* which is in the middle of the intermediate exchange regime, namely $\tau(T) \approx \tau^* = 3 \times 10^{-6}$ s for the first factor. Thus the approximate conversion between E(T) and T is

$$E(T) \approx 17.2\, k_{\mathrm{B}}T. \tag{8}$$

Thus by line shape analysis of the variable temperature ^{2}H solid-echo spectra the two cases can be distinguished.

The rest of the paper is organized as follows: First the experimental section describes the sample synthesis and preparation, the salient facts of ^{2}H solid-echo spectroscopy and the experimental details of the NMR experiments. Next the experimental results are presented, discussed and the results are summarized.

2 Experimental Section

2.1 Synthesis of MCM-41

MCM-41 was produced employing the method proposed by Gruen et al. [64]. 2.36 g of the surfactant salt (C16TAB, Aldrich) was dissolved in 9.5 g of an aqueous solution (25 %) of ammonia. 10 g of tetraethoxysilane (TEOS, Aldrich) were added at 35 °C under constant stirring. Then the solution kept at 80 °C for 72 h. The precipitated product is filtered, rinsed with distilled water, dried for 5 h at 105 °C, heated with a rate of 1 K/min to the calcinations temperature of 550 °C and then calcined.

Nitrogen isotherm curves of the MCM-41 samples studied were measured using a Gemini 2375 instrument from Micromeritics. The BET-specific surface area [50] calculated from the initial rise of the isotherm was found to be 1040 m^2/g. The pore diameter, determined from the relative pressure at the steep rise of volume adsorption according to the Dollimore and Heal formalism [65], was 3.3 nm. The adsorbed volume when the pores are completely filled gave the pore volume of 0.93 cm^3/g.

2.2 Sample Preparation

Naphthalene-d_8 (deuteration degree $\geq$98 %) was obtained from Merck, Darmstadt, and used without further purification. Before the samples were prepared, the MCM-41 was dried overnight in a Young NMR tube on a vacuum line at 10^{-5} mbar and 200 °C. After drying, 26.12 mg naphthalene-d_8 was added under an inert atmosphere in amounts corresponding to 90 % of the nominal pore volume. Then the tube was flame sealed at a length of ca. 2 cm. The sample was kept overnight at ca 200 °C in a muffle oven to ensure that all naphthalene molecules enter the pores and distribute homogeneously inside the pores.

2.3 ^{2}H NMR Solid-State NMR Spectroscopy

Molecular reorientations rotate the quadrupolar interaction tensors, which causes characteristic changes of the ^{2}H NMR line shape. The observed line shape depends strongly on the correlation time τ_c or rate constant $k = \tau_c^{-1}$ and type of the molecular motions. Depending on the rate constant, three limiting cases can be distinguished. In the slow limit $k \ll Q_{cc}$ the line shape is practically not affected. In the fast limit $k \gg Q_{cc}$, a high-temperature spectrum results, which is the average over the motional trajectory. In the intermediate exchange regime $k \approx Q_{cc}$ relatively complicated line shapes are expected, which contain detailed information about the geometry of the underlying motional process [62]. Numerical modeling of the ^{2}H-NMR spectra thus enables us to develop quantitative models of the melting process. In this modeling, the molecular reorientations are modeled as a stochastic exchange between a set of discrete molecular orientations with different quadrupolar interaction tensors. This reduces strongly the computational costs of simulating the spectra. A particularly simple modeling of the melting process is given with the

help of the five Platonic solids: tetrahedron, cube, octahedron, dodecahedron and icosahedron. The vector starting at the center of gravity of the Platonic solid and ending at one of its vertexes is regarded as the axis of a chemical bond, which corresponds to the main component of the PAS of the quadrupolar tensor. The molecular reorientations cause stochastic jumps of this vector between the different edges of the platonic solid.

All simulations were performed employing laboratory written MATLAB programs. In the simulation a pure single-spin quadrupolar Hamiltonian was assumed. Powder integration was performed employing the Koons 16,000 optimized angle set [66]: Finite pulse widths were taken into account by the formula given in Ref. [62].

2.4 Low-Temperature ^{2}H Solid-State NMR

All ^{2}H NMR spectra of the samples were measured in a homebuilt 7-Tesla solid-state NMR spectrometer described previously [67]. A standard Oxford wide bore magnet (89 mm) equipped with a room temperature shim unit was used. ^{2}H NMR pulses were generated employing a 1 kW class AB amplifier from Dressler Hochfrequenz Technik, Stolberg. To achieve a good spectral excitation, a pulse width of 3 μs for the ^{2}H nuclei was used, which is slightly shorter than the 90° pulse width. All experiments were performed using a homebuilt 5 mm NMR probe, which was placed in a dynamic Oxford CF1200 helium flow cryostat. The sample temperature was controlled by an Oxford ITC 503 temperature controller. During data acquisition the temperature was directly controlled via a Cernox sensor (Lakeshore, Westerville) placed in the direct vicinity of the sample. The temperature was stabilized over long periods (hours) before data acquisition started. All spectra were recorded using the solid-echo technique with an echo spacing of 30 μs and a full 32-step phase cycle. The number of accumulations was between 1,024 and 4,096 scans per spectrum. Before Fourier transforming the echo-signal, the phase was corrected and the imaginary part zeroed to give fully symmetric spectra.

2.5 ^{1}H Solid-State NMR Spectra

The proton magic angle spinning (MAS)-NMR spectra were measured at room temperature on a 300 MHz Varian Infinity+ three-channel solid-state NMR spectrometer, equipped with a spin-rate controller, employing a 2.5-mm dual-channel HX-MAS probe with a 90° pulse width of 1.6 μs and a rotation speed of 20 kHz.

3 Results and Discussion

Figure 2 displays the ^{1}H solid-state NMR spectrum of naphthalene at static and under MAS conditions. The line at 1.7 ppm is caused by the silanol protons [17]. From the chemical shift value it is evident that the surface is completely water free

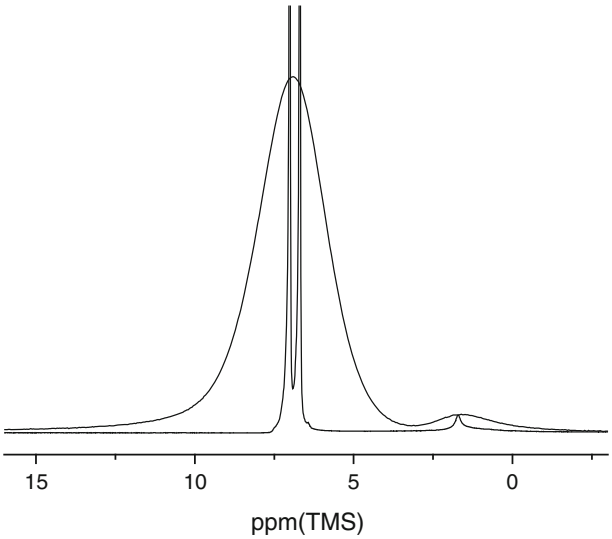

Fig. 2 Static and MAS ^{1}H-NMR spectra of naphthalene-h_8 confined inside the pores of MCM-41 with 3.3 nm pore diameter measured at room temperature

and that the silanol groups are not involved in any hydrogen bond [18, 53]. The narrow lines at 7.0 ppm and 6.7 ppm are the signals of the α-protons (see Scheme 1: 1, 4, 5, 8) and the β-protons (2, 3, 6, 7) of the naphthalene molecules.

Moreover, the chemical shift values coincide with the values observed in solution. This is a clear indication that the molecules are not stacked in the typical crystal structure, which would cause a high-field shift of the protons. Both results are characteristic for a liquid phase inside the pores.

Figure 3a shows the experimental ^{2}H NMR spectra of naphthalene-d_8 in MCM-41 (pore diameter 3.3 nm). All spectra are normalized to same height to allow for visual comparison. In reality the intensities in the spectra exhibit strong temperature dependence (see Fig. 4a; Note: to minimize the effect of noise and base-line distortions, the intensities were calculated both from the echo-amplitude and the integration of the spectrum). At low temperatures, the typical ^{2}H Pake pattern of an aromatic deuteron [56] with parameters of ($Q_{zz} = 132$ kHz, corresponding to $Q_{cc} = 176$ kHz) and ($\eta = 0.04$) is observed. These line shapes and values are typical for aromatic deuterons in a relatively rigid environment without substantial librations [39, 68]. At high temperatures a typical Lorentzian line shape is observed, which indicates that the naphthalene molecules are completely molten inside the pores and perform free isotropic reorientations. In the intermediate temperature regime line-shape changes are observed, which indicate the melting process of the naphthalene inside the pores.

It is evident that there are no visible spectral components which are indicative of a uniaxial motion in the pre-melting region, as for example C_2-flips or rotations around one of the C_2-axes of the molecule, since the latter would cause an incomplete averaging of the quadrupolar interaction. Thus we conclude that the naphthalene molecules, despite their form anisotropy, "immediately" start to perform three-dimensional motions, which average out the quadrupolar interaction to zero.

Scheme 1 Numbering of the proton/deuteron positions of naphthalene

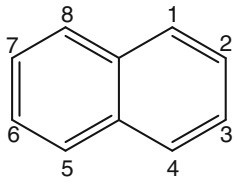

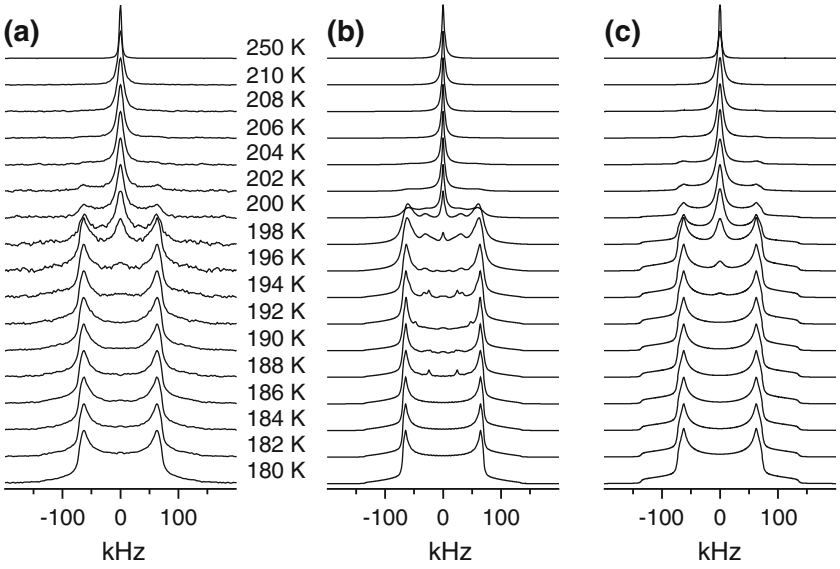

Fig. 3 Experimental (**a**) and simulated **b** octahedral jump (simulations with $k = 0.000$, 0.007, 0.008, 0.590, 1.130, 1.300, 1.450, 2.750, 7.450, 11.001, 17.349, 24.499, 28.601, 37.500, 43.499, 48.601, 80.001) kHz; **c** two-phase model) ^{2}H solid-echo NMR spectra of naphthalene-d_8 confined inside the pores of MCM-41 with 3.3 nm pore diameter. Intensities are normalized to equal height

In the case of the narrow distribution model, we employed the tetrahedral, octahedral, cubic and dodecahedral jump models geometries for the melting process. Figure 3b shows as an example the simulation employing the octahedral jump model, which gave the best reproduction of the experimental spectra, for the modeling of the melting process. However, even for this model there are strong differences in the line shapes of the spectra in the intermediate regime (198–204 K), which are most sensitive on the motional process. While the calculations predict a smearing out of the singularities at ±67 kHz), the experimental spectra exhibit pronounced singularities and resemble more closely a superposition of a low-temperature Pake spectrum and a high-temperature Lorentzian line. Moreover, there are also strong quantitative differences between calculated and experimental echo-intensities. While the experimental echo-intensities give a minimum signal of 20 %, the calculations with the different models (Fig. 4b) predict reductions to 2 % of the maximum value and a broader minimum as experimentally observed. These deviations are an indication that there is not a single melting temperature, but a distribution of melting temperatures, i.e., a disordered system.

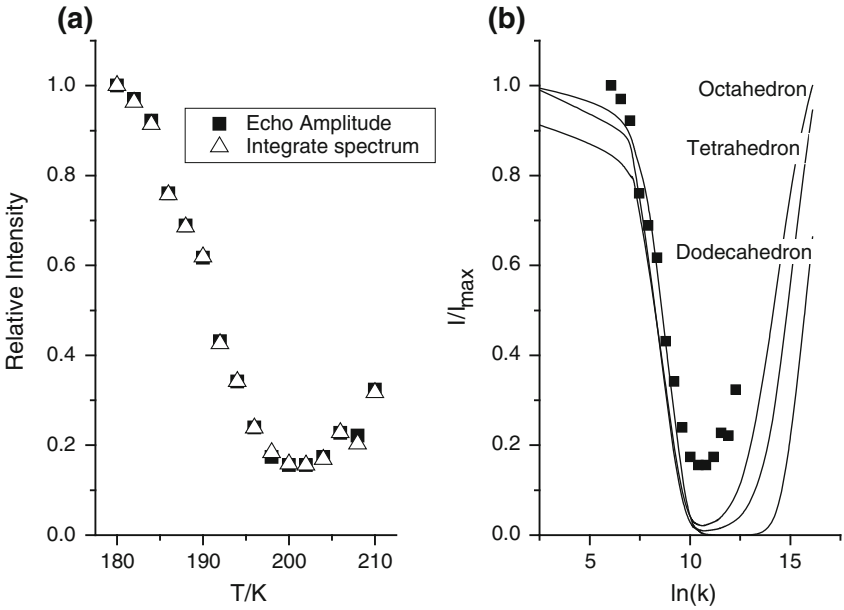

Fig. 4 **a** Relative intensities of the experimental ^{2}H solid-echo NMR signals of naphthalene-d_8 confined inside the pores of MCM-41 with 3.3 nm pore diameter as a function of temperature. **b** Comparison of the experimental intensities with the calculated echo-attenuations for different jump-models. Experimental data were converted employing an Arrhenius dependence with $E_A = 30$ kJ/mol and $A = 10^{12}$ s^{-1}

A far better agreement between experimental and simulated line shape is obtained for the case of the two-phase model (Fig. 3c). However, the simple two-phase model cannot account for the strong changes in the echo intensity, since it is based on the assumption that only a very minor part of the molecules is in the intermediate motional regime. Thus, in the following the two-phase model is employed as an empirical model to describe the observed temperature dependences, without trying to attempt to recover the distribution of activation energies from the curves.

In the two-phase model the relative areas of the Pake and the Lorentzian line are proportional to the relative concentration of the two phases. Figure 5 displays the temperature dependence of the two concentrations and their modeling employing Eq. (2). The temperature dependence of the relative concentrations is well reproduced by Eq. (2). The corresponding parameters are $T_{mid} = (201.8 \pm 0.1)$ K and $\Delta T = (4.4 \pm 0.11)$ K. Defining the mid-point where the curves intersect (50 %-point) as the effective melting point inside the pores, a value of at (201.8 ± 0.1) K is found. Comparing this value to the melting point of neat naphthalene, which is 80.3 °C, i.e., 353.4 K, shows that the melting point of the molecules inside the pores is reduced by 152 K. From the effective melting point and Eq. (8) the activation energy of the process can be estimated as $E_A = (28.8 \pm 0.1)$ kJ/mol.

It is interesting that the transition temperature distribution in Fig. 5 is narrower than those found for the melting of benzene inside SBA-15 (ref. [3], 15 K) and iso-

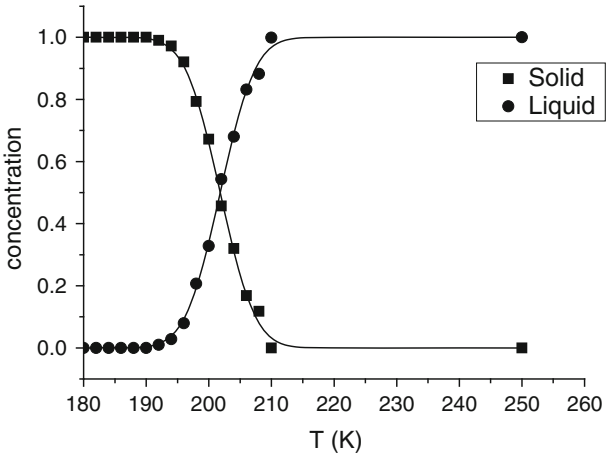

Fig. 5 Relative concentrations of the liquid- and the solid-like and their simulation employing Eq. (4). From the fits the effective melting point $T_{mid} = (201.8 \pm 0.1)$ K and the distribution width of $\Delta T = (4.4 \pm 0.11)$ K are determined

butyric acid inside MCM-41 and SBA-15 (ref. [23], 13 K, respectively 26 K), despite the larger size of the naphthalene molecule.

Comparing the results of the two-phase model and the narrow distribution model it seems evident that there is a relatively narrow distribution of melting temperatures of the naphthalene molecules inside the pores. Such a narrow distribution, however, would correspond to a, compared with other systems, relatively high degree of order of the molecules. Such a rather well-defined structure of the naphthalene molecules inside the pores could for example be the plastic crystalline phase previously proposed by Strange and co-workers [44].

4 Summary and Conclusion

The temperature dependence of the ^{2}H NMR solid-echo spectra of naphthalene molecules as guests in the mesopores of neat MCM-41 with a pore width of 3.3 nm was measured. A strong reduction of the melting point of the naphthalene molecules by 152 K is observed. The line-shape changes in the melting region were simulated with two different models, namely the model of a narrow distribution of activation energies, which is typical for a crystal like phase and a two-phase model. Both models indicate a relatively narrow distribution of melting points of the naphthalene molecules inside the pores, which is indicative of a rather well-defined structure of the naphthalene molecules inside the pores. This finding supports the proposal of a plastic crystalline phase previously proposed by Strange and co-workers [44]. A more detailed analysis of this phase would necessitate a combination of NMR measurements in a broader dynamic range, combining the deuterium line shape analysis with deuterium relaxation and spin-alignment measurements and/or

dielectric measurements with calorimetric measurements, which are beyond the scope of the present paper.

Acknowledgments Financial support by the Deutsche Forschungsgemeinschaft in the framework of the Forschergruppe FOR1583 under contract BU-911/18-1 and the state of Hessia under LOEWE SOFT-CONTROL is gratefully acknowledged.

References

1. A.I. Kitaigorodski, *Molekülkristalle* (Akademie-Verlag, Berlin, 1979)
2. E.A. Silinsh, V. Čápek, *Organic Molecular Crystals: Interaction, Localization, and Transport Phenomena* (AIP Press, New York, 1994)
3. E. Gedat, A. Schreiber, J. Albrecht, I. Shenderovich, G. Findenegg, H.-H. Limbach, G. Buntkowsky, J. Phys. Chem. B. **106**, 1977 (2002)
4. P. Medick, T. Blochowicz, M. Vogel, E. Roessler, J. Non-Cryst. Solids **307**, 565 (2002)
5. G. Dosseh, Y. Xia, C. Alba-Simionesco, J. Phys. Chem. **107**, 6445 (2003)
6. H. Jobic, Phys. Chem. Chem. Phys. **1**, 525 (1999)
7. V. Ladizhansky, G. Hodes, S. Vega, J. Phys. Chem. B , **104**, 1939 (2000)
8. Y.B. Mel'nichenko, J. Schüller, R. Richert, B. Ewen, C.-K. Loong, J. Chem. Phys. **2016**, 103 (1995)
9. L. Gjerdaker, G.H. Sorland, D.W. Aknes, Microporous Mesoporous Mater. **32**, 305 (1999)
10. A. Schreiber, H. Bock, M. Schoen, G.H. Findenegg, Mol. Phys. **100**, 2097 (2002)
11. E.W. Hansen, R. Schmidt, M. Stöcker, D. Akporiaye, Microporous Mater. **5**, 143 (1995)
12. R. Valiullin, S. Naumov, P. Galvosas, J. Kärger, H.-J. Woo, F. Porcheron, P.A. Monson, Nature **443**, 965 (2006)
13. S.A. Lusceac, C. Koplin, P. Medick, M. Vogel, N. Brodie-Linder, C. LeQuellec, C. Alba-Simionesco, E.A. Roessler, J. Phys. Chem. B **108**, 16601 (2004)
14. C. Alba-Simionesco, B. Coasne, G. Dosseh, G. Dudziak, K. Gubbins, R. Radhakrishnan, M. Sliwinska-Bartkowiak, J. Phys. Condens. Matter **18**, 15 (2006)
15. W. Masierak, T. Emmler, E. Gedat, A. Schreiber, G.H. Findenegg, G. Buntkowsky, J. Phys. Chem. B **108**, 18890 (2004)
16. E. Gedat, A. Schreiber, G. Findenegg, I. Shenderovich, H.-H. Limbach, G. Buntkowsky, Magn. Reson. Chem. **39**, 149 (2001)
17. I. Shenderovich, G. Buntkowsky, A. Schreiber, E. Gedat, S. Sharif, J. Albrecht, N.S. Golubev, G.H. Findenegg, H.H. Limbach, J. Phys. Chem. B **107**, 11924 (2003)
18. B. Grünberg, T. Emmler, E. Gedat, I. Shenderovich, G.H. Findenegg, H.H. Limbach, G. Buntkowsky, Chemistry **10**, 5689 (2004)
19. A. Vyalikh, T. Emmler, B. Grünberg, Y. Xu, I. Shenderovich, G.H. Findenegg, H.-H. Limbach, G. Buntkowsky, Z. Phys. Chem. **221**, 155 (2007)
20. S. Schemmel, D. Akcakayiran, G. Rother, A. Brûlet, B. Farago, T. Hellweg, G.H. Findenegg, Eur. Phys. J. E **12**, 1 (2003)
21. A. Vyalikh, T. Emmler, E. Gedat, I. Shenderovich, G.H. Findenegg, H.-H. Limbach, G. Buntkowsky, Solid State NMR **28**, 117 (2005)
22. S. Schemmel, G. Rother, H. Eckerlebe, G.H. Findenegg, J. Chem. Phys. **122**, 244718 (2005)
23. A. Vyalikh, T. Emmler, I. Shenderovich, Y. Zeng, G.H. Findenegg, G. Buntkowsky, Phys. Chem. Chem. Phys. **9**, 2249 (2007)
24. N. de-Sousa-Amadeu, B. Grünberg, J. Frydel, M. Werner, H.-H. Limbach, H. Breitzke, G. Buntkowsky, Z. Phys. Chem. doi:10.1524/zpch.2012.0304
25. J.M. Robertson, Proc. R. Soc. Lond. Series A **142**, 674 (1933)
26. S. Abrahams, J.M. Robertson, J. White, Acta Crystallogr. A **2**, 238 (1949)
27. S. Abrahams, J.M. Robertson, J. White, Acta Crystallogr. A **2**, 233 (1949)
28. D. Cruickshank, Acta Crystallogr. A **10**, 504 (1957)
29. S. McGuigan, J.H. Strange, J.M. Chezeau, Mol. Phys. **49**, 275 (1983)
30. J.U. vonSchütz, H.C. Wolf, Z. Naturforsch., A: Phys. Sci. **27**, 42 (1972)
31. G. Maier, U. Haeberlen, H.C. Wolf, Phys. Lett. **25a**, 323 (1967)
32. G. Maier, U. Haeberlen, H.C. Wolf, K.H. Hausser, Phys. Lett. **25a**, 384 (1967)

33. H. Vieth, V. Macho, D. Stehlik, J. Phys. Chem. **83**, 3435 (1979)
34. J. Allgeier, V. Macho, D. Stehlik, H.M. Vieth, W. Auch, J.U. von Schuetz, Chem. Phys. Lett. **86**, 522 (1982)
35. G. Buntkowsky, M. Nack, D. Stehlik, H.M. Vieth, Isr. J. Chem. **29**, 109 (1989)
36. J. Allgeier, G. Buntkowsky, S. Hentrich, W. Hoffmann, H.M. Vieth, Isr. J. Chem. **32**, 205 (1992)
37. G. Buntkowsky, K. Salikhov, D. Stehlik, H.M. Vieth, J. Phys. Condens. Matter **3**, 6093 (1991)
38. G. Buntkowsky, W. Hoffmann, T. Kupka, G. Pasternad, M. Jaworska, H.M. Vieth, J. Phys. Chem. A. **102**, 5794 (1998)
39. G. Buntkowsky, W. Hoffmann, H.M. Vieth, Appl. Magn. Reson. **17**, 489 (1999)
40. M. Ebener, G. Vonfircks, H. Günther, Helv. Chim. Acta **74**, 1296 (1991)
41. M. Ebener, V. Francke, H. Günther, Fresenius' J. Anal. Chem. **357**, 505 (1997)
42. G. von Fircks, H. Hausmann, V. Francke, H. Günther, J. Org. Chem. **62**, 5074 (1997)
43. H. Günther, S. Oepen, M. Ebener, V. Francke, Magn. Reson. Chem. **37**, 142 (1999)
44. J. Mitchell, J. Strange, Mol. Phys. **2004**, 102 (1997)
45. J.A. Lee, H. Rösner, J.F. Corrigan, Y. Huang, J. Phys. Chem. C. **115**, 4738 (2011)
46. J.S. Beck, J.C. Vartuli, W.J. Roth, M.E. Leonowicz, C.T. Kresge, K.D. Schmitt, C.T.W. Chu, D.H. Olson, E.W. Sheppard, S.B. Mccullen, J.B. Higgins, J.L. Schlenker, J. Am. Chem. Soc. **114**, 10834 (1992)
47. J.P. Gabaldon, M. Bore, A.K. Datye, Top. Catal. **44**, 253 (2007)
48. G. Oye, J. Sjöblom, M. Stöcker, Adv. Colloid Interface Sci. **89**, 439 (2001)
49. A. Sayari, Stud. Surf. Sci. Catal. **102**, 1 (1996)
50. S. Brunauer, P.H. Emmett, E. Teller, J. Am. Chem. Soc. **60**, 309 (1938)
51. B. Kuchta, L. Firlej, R. Denoyel, P. Boulet, S. Rols, M. Johnson, Appl. Surf. Sci. **253**, 5601 (2007)
52. C. Sonwane, S. Bhatia, N. Calos, Langmuir **15**, 4603 (1999)
53. G. Buntkowsky, H. Breitzke, A. Adamczyk, F. Roelofs, T. Emmler, E. Gedat, B. Grünberg, Y. Xu, H.H. Limbach, I. Shenderovich, A. Vyalikh, G.H. Findenegg, Phys. Chem. Chem. Phys. **9**, 4843 (2007)
54. A. Gruenberg, H. Breitzke, G. Buntkowsky, Spectrosc. Prop. Inorg. Organomet. Compd. **43**, 289 (2012)
55. C. Favire, D. Bellet, G. Dolino, Eur. Phys. J. B. **7**, 19 (1999)
56. R. Hentschel, H.W. Spiess, J. Magn. Reson. **35**, 157 (1969)
57. C. Schmidt, S. Wefing, B. Blümich, H. Spiess, Chem. Phys. Lett. **130**, 84 (1986)
58. C. Schmidt, B. Blumich, H.W. Spiess, J. Magn. Reson. **1988**(79), 269 (1969)
59. A. Hagemeyer, K. Schmidt-Rohr, H.W. Spiess, Adv. Magn. Reson. **13**, 85 (1989)
60. R.R. Vold, in *Nuclear Magnetic Resonance Probes of Molecular Dynamics,* ed. by R. Tycko (Kluwer Academic Publishers, Dordrecht, 1994) p. 27
61. C.P. Slichter, *Principles of Magnetic Resonance*, 3rd edn. (Springer, Berlin, 1990)
62. K. Schmidt-Rohr, H.W. Spiess, *Multidimensional Solid State NMR and Polymers* (Academic Press, London, 1994)
63. E. Roessler, M. Taupitz, K. Börner, M. Schulz, H.M. Vieth, J. Chem. Phys. **92**, 5847 (1990)
64. M. Gruen, K.K. Unger, A. Matsumoto, K. Tsutsumi, Microporous Mesoporous Mater. **27**, 207 (1999)
65. D. Dollimore, G.R.J. Heal, Appl. Chem. **14**, 109 (1964)
66. J.M. Koons, E. Hughes, H.M. Cho, P.D. Ellis, J. Magn. Res. A **114**, 12 (1995)
67. F. Wehrmann, J. Albrecht, E. Gedat, G.J. Kubas, H.H. Limbach, G. Buntkowsky, J. Phys. Chem. A **106**, 2855 (2002)
68. J.H. Ok, R.R. Vold, R.L. Vold, M.C. Etter, J. Phys. Chem. **93**, 7618 (1989)